Astron. Astrophys. 333, 141–150 (1998)

ASTRONOMY AND ASTROPHYSICS

Towards a seismic model of the δ Scuti star XX Pyxidis

A.A. Pamyatnykh[1,2,3], **W.A. Dziembowski**[1,2], **G. Handler**[2], **and H. Pikall**[2]

[1] N. Copernicus Astronomical Center, Polish Academy of Sciences, Bartycka 18, PL-00716 Warszawa, Poland
[2] Institute of Astronomy, University of Vienna, Türkenschanzstraße 17, A-1180 Wien, Austria
[3] Institute of Astronomy, Russian Academy of Sciences, Pyatnitskaya 48, 109017 Moscow, Russia

Received 26 November 1997 / Accepted 26 January 1998

Abstract. Frequencies of 13 oscillation modes in the star XX Pyxidis (CD–24 7599) are accurately measured but for none of the modes the spherical harmonic degree (ℓ) is known. We present results of an attempt to construct the model whose low–ℓ mode frequencies reproduce possibly close the observations. Models are constrained by the mean photometric and spectroscopic data for the star. However, the strongest constraint on the effective temperture is from the requirement that the modes excited in the star fall into the range of the modes driven by the opacity mechanism.

Our models are built with the standard stellar evolution code allowing no overshooting from the convective core. Effects of rotation are taken into account both in stellar evolution and in linear nonadiabatic oscillation calculations. Uniform rotation rate and conservation of the global angular momentum during evolution are assumed.

We find several distinct mode identifications and associated stellar models leading to frequency fits of similar quality. Determination of the ℓ values for some of the modes could remove the ambiguity. None of the fits is satifactory: the mean departures exceed the mean observational frequency error by at least one order of magnitude. The fits could be improved by means of adjusting model parameters that were kept fixed. However, such effort will be meaningful only after improving accuracy in calculation of the effects of rotation in oscillation frequencies.

Key words: stars: oscillations – stars: evolution – δ Scu – stars: individual: CD–24 7599 = XX Pyx

1. Introduction

Long–time network observations of Delta Scuti stars resulted in establishing truly multimodal character of oscillations in a few objects of this type. The four objects with the largest number of modes detected are FG Virginis with 24 modes (Breger et al. 1997), 4 Canum Venaticorum with at least 17 modes (Breger 1997), XX Pyxidis with 13 modes (Handler et al. 1997a) and BH Piscium with 13 modes (Mantegazza et al. 1996). Though these numbers of modes in comparison with the Sun or certain oscillating white dwarfs may appear small, reproducing mode frequencies with model calculation represents a challenge.

What makes our task more difficult than in the solar and white–dwarf cases, is the fact that the observed spectra do not reveal patterns enabling mode identification. Modes detected in δ Scuti stars are of low radial order and their frequencies do not obey simple asymptotic relations. Further, these stars are rather rapid rotators and rotational splitting is not equidistant. Multicolor photometry may be used to determine the spherical harmonic degree, ℓ. Spectroscopy allows, in addition, to determine the azimuthal order, m. In practice, however, reliable ℓ and m values are only seldom available. Thus, mode identification in δ Scuti stars cannot be done independently of calculations involving construction of equilibrium models and their oscillation properties. The aim is to construct a stellar model with frequencies of low–degree modes which fit the observed ones. In analogy to helioseismology we use the name *seismic model*.

The ultimate purpose of seismic model construction is testing the ingredients of stellar evolution theory: its basic assumptions and the input microscopic physics. Stellar evolution theory has reached an advanced level some 20 to 30 years ago. However, important questions concerning convection and rotation remain unanswered. For instance, is the mixing–length theory sufficient for describing convective flux in subphotospheric layers? If so, what is the best choice for the mixing length parameter, α, depending on stellar parameters? What is the extent of element penetration, $d_{\rm over}$, from the convective to the radiative regions? What is the law of the angular momentum evolution? What is the role of rotationally induced instabilities in chemical element mixing?

In recent years considerable progress has been made in treatment of the equation of state and opacity for stellar interiors (see Christensen–Dalsgaard & Däppen 1993 and references there, Rogers et al. 1996, Rogers & Iglesias 1994 and references there, Iglesias & Rogers 1996, Seaton 1996). The uncertainties, however, are difficult to estimate. It is therefore important to use possibly diversified sets of observational data for testing. Observers provide us very accurate frequency measurements but a major effort is needed to connect these quantities to other stellar characteristics and to parameters used in model construction.

In the next section we will outline methodology of constructing seismic models, which, we believe, is applicable to all

Send offprint requests to: W.A. Dziembowski

multimode δ Scuti stars in the Main Sequence phase of evolution. We should stress that our work is not the first effort aimed at reproducing observed frequencies in objects of this type. Goupil et al. (1993) modelled GX Pegasi for which five frequencies have been measured. Breger et al. (1995) and Guzik and Bradley (1995) constructed models of FG Virginis, which approximately reproduced observations. Our target accuracy is much higher – we want to approach the level of the observational error.

The rest of this paper concerns XX Pyxidis (CD–24 7599), which seemed to be a good choice for the first attempt in accurate reproducing observed spectrum. Amongst most multimode δ Scuti stars it is the hottest and least evolved. In such stars the predicted spectrum of unstable modes is relatively simple. With the progress of stellar evolution the instability extends to mode of mixed pressure/gravity (p/g) character and to pure g–modes. Separations in frequency between modes of the same $\ell > 0$ decrease, which complicates mode identifcation. In post Main Sequence stars the density of predicted spectra is so high that the task of mode identification will remain impossible unless we discover the clue to mode selection. Furthermore, the uncertainty in the description of the subphotosperic convection is less severe in this relatively hot star.

After presenting data in Sect. 3, we discuss in Sect. 4 constraints on mean parameters of the star. The methodology of the simultaneous search for mode identification and refinement of model parameters is described in Sect. 5. In the same section several alternative solutions are presented. In Sect. 6 we explain why these are unreliable and in the last section we discuss prospects for construction of a still improved seismic model of the star.

2. Construction of seismic stellar models

2.1. Principles

The number of modes detected in individual δ Scuti stars is far too small to attempt to determine radial structure directly from measured frequencies. Everything we may hope to achieve is to use the observed frequencies to determine global parameters characterizing the star and certain parameters of the theory. The equations of problem are obtained by equating observed and calculated frequencies,

$$f_{j,\mathrm{obs}} = f_{j,\mathrm{cal}}(\ell_j, m_j, n_j, \boldsymbol{P}_S, \boldsymbol{P}_T), \quad (1)$$

where j labels measured frequencies, ℓ_j, m_j, n_j are numbers identifying the mode, $\boldsymbol{P}_S$ gives the set parameters characterizing the model, and $\boldsymbol{P}_T$ gives the set of free parameters of the theory.

A comment is needed about n_j. Nonradial modes excited in δ Scuti stars could be p–modes, g–modes, and modes of mixed character. In the present application, continuity of f as function of $\boldsymbol{P}$ for specified (ℓ, m, n) is essential. The avoided crossing effect causes that the continuity is guaranteed if we define the n values at ZAMS where the g– and p–mode spectra are separated in frequency. Following Unno et al. (1989) we will denote with $n < 0$ and $n > 0$ modes which in ZAMS models are consecutive g– and p–modes, respectively. For $\ell > 1$ there is the fundamental mode which is denoted with $n = 0$. With this choice, in evolved models some of modes denoted with $n > 0$ will have predominatly g–mode properties and *vice versa*.

The parameters given by $\boldsymbol{P}_S$ are those characterizing the evolutionary sequence like initial mass M, chemical composition, X_0 and Z_0, and the angular momentum. In addition, there is a single parameter identifying the model within the evolutionary sequence. The age is always a good choice. In the present application we use the initial equatorial velocity $V_{\mathrm{rot},0}$ instead of the angular momentum and $\log T_{\mathrm{eff}}$ instead of the age. The latter choice is acceptable because XX Pyx is certainly in the expansion phase of the Main Sequence evolution and T_{eff} is a monotonic function of the age. In any case there are five parameters in $\boldsymbol{P}_S$.

The quantities one may include in $\boldsymbol{P}_T$ are mixing–length parameter α, overshooting distance d_{over}, as well as parameters characterizing angular momentum evolution and mass loss. None of these will be included in the present work. Constraining these parameters is certainly the most important application of asteroseismology. However, as we will see later in this paper, we are not yet at this stage.

2.2. Tools

2.2.1. Evolution code

Stellar evolution code we use was developed in its original version by B. Paczyński, R. Sienkiewicz and M. Kozlowski. It is in fact a modern version of B. Paczyński's code (Paczyński 1969, 1970), which is now written in a modular form enabling an easy implementation of microscopic physics data from various sources. In the present application we use most recent versions of OPAL opacity (Iglesias & Rogers 1996) and equation of state (Rogers et al. 1996) data. The nuclear reaction rates are the same as used by Bahcall and Pinsonneault (1995).

The effect of averaged centrifugal force is taken into account in the equation for hydrostatic equilibrium. We assume uniform rotation and conservation of global angular momentum. These are the simplest assumptions which we are prepared to abandon if this is required for a successful seismic model construction. Similarily, we are prepared to introduce overshooting and/or rotationally induced mixing of the chemical elements outside of the convective core, but these effects are ignored in the present work. With these assumptions the input parameters for sequences are total mass, M, initial values for hydrogen abundance, X_0, metal abundance, Z_0, and the equatorial velocity $V_{\mathrm{rot},0}$. Initial heavy element mixture is that of Grevesse & Noels (1993). The assumed parameters for convection are $\alpha = 1$, $d_{\mathrm{over}} = 0$. The choice of α is unimportant in the present application.

For selected values of T_{eff} the code returns all needed parameters of the model such as $\log g_{\mathrm{eff}}$, V_{rot} or Ω and the matrix of the coefficients needed for calculation of linear nonadiabatic oscillation properties.

2.2.2. Nonadiabatic oscillation code

The code we use is a modified version of the code developed long ago by one of us (Dziembowski 1977). The important modification is taking into account the effect of the averaged centrifugal force. Modified equations for adiabatic oscillations are given by Soufi et al. (1997). The corresponding change in the full nonadiabatic set is trivial. The input to this code specifies the range of frequencies and the maximum value of ℓ. The standard output are the following characteristics of the $m = 0$ modes: complex dimensionless frequencies σ, modified growth rates, η, and the complex ratio of the flux to displacement eigenfunctions at the surface, $\mathcal{F}$.

The frequency, f, which we compare with observations is given by the real part of σ:

$$f = \Re(\sigma)\sqrt{\frac{G\bar{\rho}}{\pi}}. \quad (2)$$

For higher order p–modes beginning with, say, $n = 5$ or 6, the nonadiabatic effects are important at the level of the accuracy of frequency measurements. The growth rate is given by $-\Im(\sigma)$. A more convenient measure of mode stability is η which varies from -1, if damping occurs everywhere in the stellar interior, to $+1$, if driving occurs everywhere. At neutral stability we have $\eta = 0$. Values of η are important as constraints on modes and models. We will use them in the next sections. Also $\mathcal{F}$'s have applications in asteroseismology, especially, in determination of ℓ–values (see Cugier et al. 1994). However, we do not have neccesary observational data on XX Pyx to make use of this quantity.

2.2.3. Calculation of the rotational splitting

Rotation has an important effect on the structure of oscillation spectra. Even at modest equatorial velocities such as 50–100 km/s the effect of rotation can not be reduced to the linear splitting $\propto m\Omega$. Our code calculating the rotational splitting is accurate up to Ω^2. It is a version of the code by Dziembowski and Goode (1992) modified by two of us (WAD, AAP) and M.–J. Goupil. It uses the adiabatic approximation. The same nonadiabatic correction evaluated with the the code described in the previous subsection is added to all modes within the multiplet.

3. Frequency data

More than 350 hours of time–series photometric observations of XX Pyx are available. These include two Whole Earth Telescope runs (Handler et al. 1996, 1997a) as well as follow–up measurements to study the star's amplitude and frequency variations (Handler et al. 1997b).

Analysis of the two WET data sets allowed the extraction of 13 pulsation frequencies plus one 2f–harmonic. These frequencies are summarized in Table 1, and mostly taken from Handler et al. (1997a, hereafter HPO). Moreover, from an examination of the follow–up data, the values of frequencies f_1, f_2 and f_3 could be refined. The three revised frequencies are also listed in Table 1. Their error sizes differ from those listed in HPO, since these frequencies are now known without alias ambiguity. However, these three frequencies are slightly variable (Handler et al. 1997b). Therefore the error bars have been modified to account for the latter effect.

Table 1. Frequencies of the 13 pulsation modes and the $2f_1$–harmonic of the δ Scuti star XX Pyx unambiguously detected by HPO

	Frequency (cycles/day)	Ampl. (1992) (mmag)	Ampl. (1994) (mmag)
f_1	38.1101 ± 0.0004	11.5 ± 0.2	15.9 ± 0.2
f_2	36.0113 ± 0.0010	10.0 ± 0.2	3.3 ± 0.2
f_3	33.4370 ± 0.0002	6.4 ± 0.2	3.8 ± 0.2
f_4	31.3925 ± 0.0025	3.8 ± 0.2	1.9 ± 0.2
f_5	28.9950 ± 0.0025	2.4 ± 0.2	2.7 ± 0.2
f_6	27.0028 ± 0.0025	2.4 ± 0.2	1.6 ± 0.2
f_7	34.6657 ± 0.0038	2.2 ± 0.2	2.0 ± 0.2
f_8=$2f_1$	76.2203 ± 0.0038	0.8 ± 0.2	1.1 ± 0.2
f_9	27.2635 ± 0.0138	1.0 ± 0.2	1.9 ± 0.2
f_{10}	29.6196 ± 0.0075	1.5 ± 0.2	1.3 ± 0.2
f_{11}	33.6367 ± 0.0125	1.2 ± 0.2	1.7 ± 0.2
f_{12}	28.6980 ± 0.0138	1.1 ± 0.2	1.5 ± 0.2
f_{13}	31.2033 ± 0.0163	1.4 ± 0.2	1.1 ± 0.2
f_{14}	31.9062 ± 0.0100	1.0 ± 0.2	1.7 ± 0.2

4. Constraints

4.1. Mean surface parameters from observations

To estimate the position of XX Pyx in the H–R diagram, color photometry and high–resolution spectroscopy of the star have been carried out by HPO. Applying calibrations to the photometric data, they infer that XX Pyx is a main–sequence δ Scuti star with $T_{\rm eff} = 8300 \pm 200$ K, $\log g = 4.25 \pm 0.15$. From their spectroscopy HPO determined the star's projected rotational velocity with $v \sin i = 52 \pm 2$ km/s and that the object has approximately solar metal abundance: $[M/H] = 0.0 \pm 0.2$.

4.2. Structures in the power spectra

An important constraint for identifying the different pulsation frequencies of XX Pyx with the corresponding quantum numbers was found by HPO. They searched for characteristic spacings within the 13 pulsation frequencies with a Fourier technique: they assumed unit amplitude for all the individual pulsations they detected and Fourier analysed the resulting signal. This is analogous to a spectral window: the power spectrum of such a signal has maxima at the sampling frequency and its harmonics (see Kurtz 1983). With this method it is possible to find regular frequency spacings in an objective way.

There are two physical reasons why regular frequency spacings can be present: in case of slow (rigid) rotation the members of different multiplets are approximately equally spaced in frequency. Since the measured $v \sin i$ of XX Pyx is 52 km/s (HPO), rotational splitting could, under favourable circumstances, be

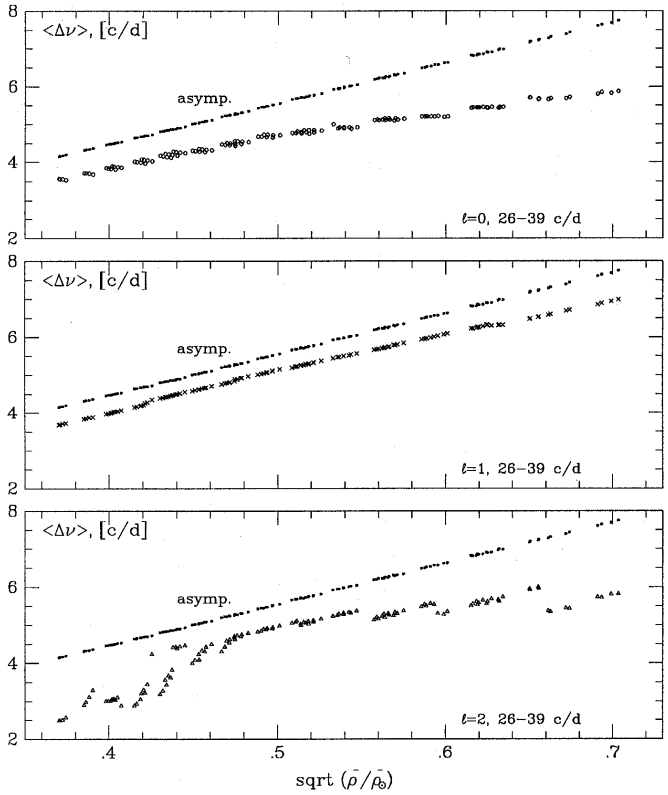

Fig. 1. Asymptotic frequency spacing of high-order p–modes of our main–sequence models compared to the mean spacing of ℓ = 0, 1, 2 modes in the frequency range excited in XX Pyx. Only axisymmetric ($m = 0$) modes are shown. Rightmost points correspond to stellar models of lowest mass and highest effective temperature. The higher mass and/or the lower effective temperature the higher overtones of p–modes are appeared in a fixed frequency range, therefore the mean frequency spacing is approaching the asymptotic value. The scatter of the datapoints, most pronounced for $\ell = 0$ modes, reflects the different rotation rates of our models. The discontinuities of $\ell = 2$ modes at $\sqrt{(\bar{\rho}/\bar{\rho}_\odot)} \leq 0.46$ are due to intruding g–modes, while more regular level shifts of $\ell = 1$ and $\ell = 2$ modes are caused by different overtones (and different number of these overtones) appearing in the frequency range of interest.

detected. The second possibility is that consecutive modes of the same ℓ are excited. Even for low–overtone pulsations such modes are approximately equally spaced in frequency.

To illustrate this second possibility, we used our basic grid of the main–sequence models and their oscillation frequencies (see Subsect. 5.2): $M = 1.75 - 2.05\ M_\odot$ with a step of $0.05\ M_\odot$, $\log T_{\rm eff} = 3.905 - 3.925$ with a step of 0.05, $V_{\rm rot,0} = 50 - 125$ km/s with a step of 25 km/s. For each of these models, we compared the asymptotic frequency spacing with the mean spacing between frequencies of consecutive modes of a given ℓ value. We restrict to the observed frequency range of XX Pyx. The results are shown in Fig. 1. (Remember that the asymptotic frequency spacing for high overtone p–modes is determined by the following formula, see Unno et al. 1989, Eq. (16.36): $\Delta\nu = 0.5/(\int_0^R \frac{dr}{c})$, where c is the sound speed, — i.e. it is proportional to the square root of the star's mean density.)

As can easily be seen from Fig. 1, the assumption that regular frequency spacings are present even at relatively low overtones is justified. The frequency spacings of the different ℓ's are very similar. Consequently, HPO carried out the Fourier analysis described above and discovered a regular frequency spacing within the pulsation modes of XX Pyx, with a probability of less than 3% that this detection was caused by chance. Because of the value of this spacing ($\approx 26\ \mu$Hz ≈ 2.25 c/d), HPO suggested that it cannot reflect rotational splitting (since the second–order terms would destroy any frequency symmetry at such high rotation rates).

From a comparison of the Fourier analyses of the observed and of several model frequency spectra, HPO concluded that this spacing is caused by the presence of modes corresponding to consecutive overtones of $\ell = 1$ and $\ell = 2$ modes. HPO determined the spacing of consecutive overtones of the *same* ℓ with $54.0 \pm 2.3\ \mu$Hz ($= 4.67 \pm 0.20$ c/d). This frequency spacing is a measure of the sound crossing time through the object, and thus it can be used to determine the mean density of the star. For a model sequence with solar metallicity, HPO determined $\bar{\rho} = 0.246 \pm 0.020\ \bar{\rho}_\odot$.

HPO performed several tests to verify the validity of this method and the correct interpretation of its result (see their paper for more details) and found their Fourier technique to be reliable, since the frequency spectrum of XX Pyx is very well suited for such an analysis: only a few overtones are excited, but a large number of possible pulsation modes are photometrically observed.

Actually, one can use this Fourier method to test a common assumption in mode identification attempts from photometric (and radial velocity) data: with increasing degree ℓ of the pulsations, geometrical cancellation (Dziembowski 1977, Goupil et al. 1996) decreases the photometric amplitude of the modes. Therefore, it is usually assumed that only modes with $\ell < 3$ can be detected using photometric data. The photometric amplitude of an $\ell = 3$ mode with the same intrinsic amplitude as an $\ell = 1$ mode is only about a factor of 12 smaller, which is approximately the range of photometric amplitudes of the different pulsation modes detected for XX Pyx. However, when considering rotational splitting, seven modes of $\ell = 3$ can be present, but only three $\ell = 1$ modes. Therefore it can not be ruled out that a non–negligible number of $\ell = 3$ modes is excited to observable amplitude.

Consequently, we applied HPO's Fourier technique to model frequencies, incorporating modes with $\ell = 3$ and/or $\ell = 4$. In cases where many of these high ℓ modes were present, no significant frequency spacing could be found, since their rotationally split patterns "masked" the regular spacing of the $\ell = 0 - 2$ modes. Only with a few of the high ℓ modes the typical frequency spacing could be revealed. This suggests that most of the pulsation modes of XX Pyx are indeed of $\ell = 0 - 2$.

4.3. Implication from the stability survey

XX Pyx is a hot δ Scuti star located near the blue edge of the instability strip. In such an object the opacity mechanism driving

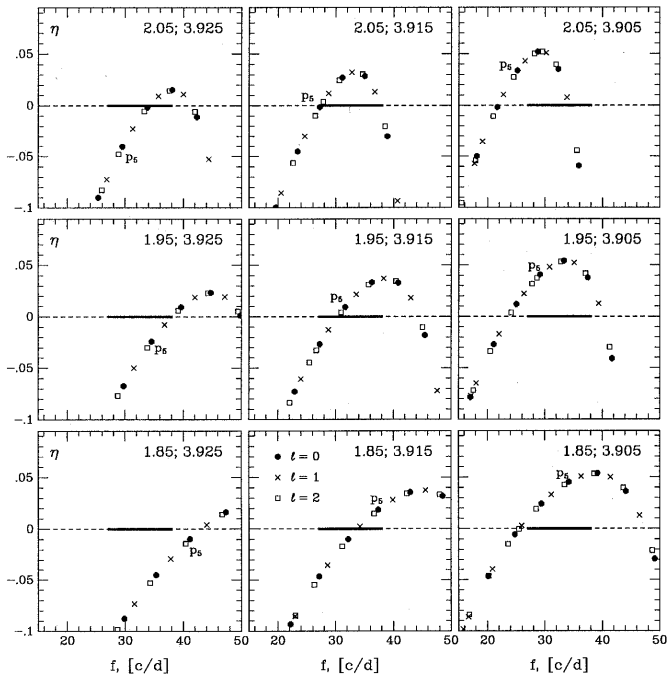

Fig. 2. Normalized growth rates, η, plotted against frequency, f, in selected models spanning the allowed ranges of M and $\log T_{\rm eff}$. The values of M (in solar units) and $\log T_{\rm eff}$ are given in each panel. Models were calculated with $X_0 = 0.7$, $Z_0 = 0.02$ and $V_{\rm rot} = 0$. The symbol $\rm p_5$ is plotted near the corresponding radial overtone. The thick horizontal line shows the range of frequencies measured in XX Pyx.

is confined to modes in a narrow range of frequencies and the driving effect is marginal. This is seen in Fig. 2. Values of η never exceed 0.05. The range of f where $\eta > 0$ never spans more than three radial orders for radial modes. In models considered the lowest values of n is 4 and the highest is 8. The behaviour of $\eta(f)$ in several models is shown in Fig. 2. The selected models have the surface parameters in the range consistent with the data on XX Pyx. The independence on ℓ and occurence of a single maximum are typical features for the opacity driven modes.

Values of η do not have the same reliability as those of f. Our treatment of the optically thin layers and the convective flux is crude. Therefore we will regard identifications with modes of small negative η's as admissible. However, we can exclude identifications involving radial modes with $n < 4$ and $n > 8$ as well we can exclude all models with, approximately, $\log T_{\rm eff} > 3.925$ and the low mass models with $\log T_{\rm eff} > 3.92$ (see Fig. 2).

5. A search for best parameters and mode identification

We have no observational information about the ℓ and m values for the modes detected in XX Pyx. The assignment of these two quantum numbers as well as n may only be done together with model parameter determination. The basis is Eq. (1) applied to the 13 measured frequencies. We only assume that all modes are of low degree. Most of the results we will present here were obtained with the assumption $\ell \leq 2$ for all modes. We carried out also calculation allowing one of the mode to have $\ell = 3$. Some of the results for such a case will be discussed at the end of this section.

At this stage we allow no free theoretical parameters $\boldsymbol{P}_T$ and we fix X_0 and Z_0 at the values 0.7 and 0.02, respectively. Thus, we allow only three free model parametres: M, $V_{\rm rot,0}$, and $T_{\rm eff}$. For each model the modes are assigned to minimize

$$\chi^2 = \tfrac{1}{j}\sum_{i=1}^{j}(f_{{\rm obs},i} - f_{{\rm calc},i})^2, \qquad (3)$$

where $j = 13$ or 12. The first value was used in the case when we assumed $\ell \leq 2$ for all modes. In the alternative version we search for the minimum of χ^2 relaxing the fit for one of measured frequency. In the automatic fitting routine we made sure that each of the model frequencies was assigned at most to one of the stellar frequencies.

5.1. Uncertainties in stellar and model frequencies

In our search for best models and mode identification we use unweighted observational data. The reason is that the errors in the frequency measurements are smaller than the uncertainities in the theoretical values. In Table 1 we may see that the errors range from 4×10^{-4} for f_1 to 163×10^{-4} for f_{13}. Thus the relative accuracy of frequency is, at worst, $\sim 5 \times 10^{-4}$, which is by one order of magnitude less than the theoretical uncertainty.

The main problem on the side of theory is in the treatment of rotation. We found that at equatorial velocities ~ 100 km/s the second order perturbation treatment yields relative accuracy in frequencies $\sim 5 \times 10^{-3}$.

5.2. Tabulation of model frequencies

With the codes described in Subsect. 2.2 we prepared tables with frequencies for modes with $\ell = 0$, 1, 2 covering the range of the stellar pulsation frequencies. At this stage we neglected the effects of near–degeneracy which we discuss in Sect. 6, because it complicates calculations and it is not essential at this stage. The range of $\log T_{\rm eff}$ values was $[3.905 - 3.925]$ with a step of 0.05. The lower limit is somewhat less than the lower limit allowed by the photometry (Subsect. 4.1) while the upper limit follows from the stability consideration (Subsect. 4.3). The range of equatorial velocities was $[50 - 125]$ km/s with a step of 25 km/s. Here the lower limit follows from the $v \sin i$ measurement (Subsect. 4.1). The upper limit was adopted to avoid large errors in treatment of rotation. The adopted mass range was $[1.75 - 2.05] M_\odot$ with a step of $0.05 M_\odot$. The implied range of the mean density is significantly larger than that inferred in Subsect. 4.2. We consider models in the wider range of mean densities because there is a nonzero probability that the HPO spacing is caused by chance.

5.3. Properties of $\chi^2(M, V_{\rm rot,0}, T_{\rm eff})$

We calculated values of χ^2 according to Eq.(3) with $j = 13$ for nearly 40000 models interpolating model parameters and frequencies from the three–dimensional basic grid described

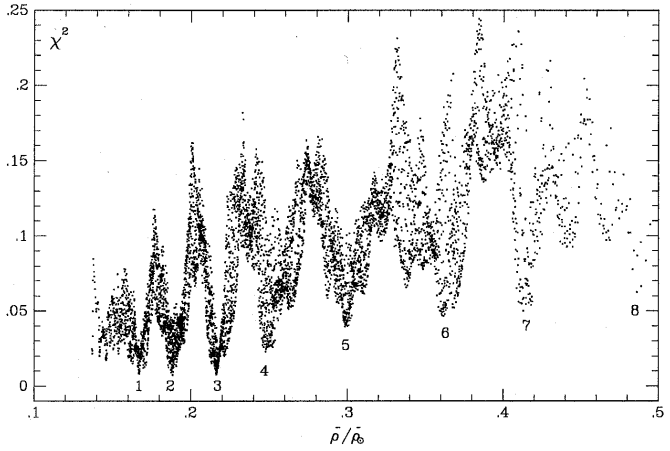

Fig. 3. Values of χ^2 evaluated for frequencies in ~ 7000 models in the ranges $M = 1.75 - 2.05\ M_\odot$, $V_{\rm rot,0} = 50 - 110$ km/s, $\log T_{\rm eff} = 3.905 - 3.925$. The patterns are the same (but less dense) as in the case of ~ 40000 models used to choose best identifications.

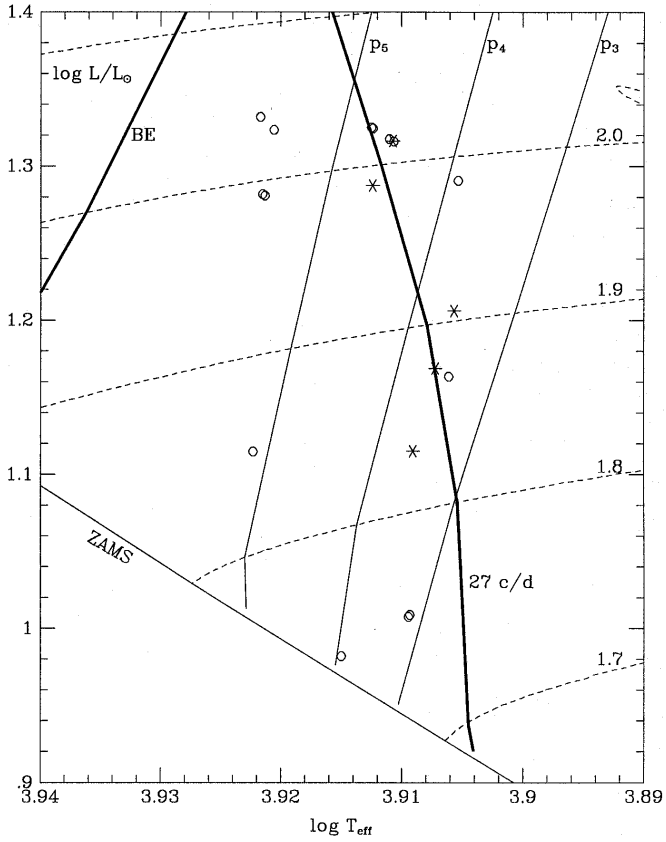

Fig. 4. Position (symbols) of the best models in the H–R diagram. The asterisks show the models used in Fig. 5. The evolutionary tracks for models with indicated mass and $V_{\rm rot} = 0$ are shown with dashed lines. The line denoted with BE shows the absolute blue edge; there are no unstable modes in models to the left of this line. The lines denoted with p_n are the blue edges for the corresponding radial overtones and the line denoted with 27 c/d is the blue edge for modes with the corresponding frequency.

above. At this stage we confined the upper limit of the equatorial rotational velocity still more, to the value of 110 km/s. In Fig. 3 we plot the values of χ^2 against mean density, which is the most important parameter determining p–mode spectra. We see several dips in χ^2 which allows us to isolate potential mode identification. One of the dips occurs close to $\bar\rho = 0.246$, which was the preferred value from the observational frequency spacing. The present analysis shows that there are few alternative "good" values. We stress that a good fit may occur even if there is no preferred spacing. The coincidence however speaks in favor of identfications corresponding to this particular dip. The dips become shallower with the increasing $\bar\rho$ which merely reflects the fact that in less evolved models there are fewer modes in the specified frequency range.

At this stage we have to consider the identifications associated with the dips located near the following eight values of $\bar\rho$: 0.17, 0.19, 0.22, 0.25, 0.30, 0.36, 0.41 and 0.49. It should be noted, however, that all the minimum values of χ^2 are still far larger than the measurement errors.

Next important parameter is the equatorial velocity of rotation which determines the m–dependence. The plot of χ^2 against $V_{\rm rot,0}$, which we do not reproduce here, shows two shallow minima around the values 60 and 100 km/s.

5.4. Possible models and identifications

There is no doubt that if all (or almost all) 13 modes detected in XX Pyx are of $\ell \le 2$ degree then the mode identification and model must correspond to one of the dips in χ^2. At each dip we chose a number of identifications with nearly the same lowest values of χ^2. All such identifications are listed in Table 2. They are grouped according to the dips. For each specified identification the three model parameters – M, $V_{\rm rot,0}$, $\log T_{\rm eff}$ – are determined through the χ^2 minimalization. These and other model characteristics are listed in Table 3.

Not all models listed in Table 3 are consistent with the requirement that the identified modes are pulsationally unstable. Thus far we made a limited use of the constraint following from the stability considerations.

In fact, the stability argument may be used to eliminate some of the models listed in Tables 2 and 3 as candidates for the seismic model of XX Pyx. A comparison of the model positions with the blue edges in the H–R diagram, shown in Fig. 4, facilitates the elimination. We see that all the models with $M \le 1.9 M_\odot$ and hotter than some $\log T_{\rm eff} = 3.91$ lie rather far from the blue edge for modes with $f \le 27$ c/d, which is the lowest frequency observed in XX Pyx. At higher masses the upper limit of $\log T_{\rm eff}$ should be moved to 3.914. In this way we may eliminate models D2B, D2C, D3B, D3C and D8A.

Perhaps model D1A may be eliminated with the opposite argument because it lies far to the red of the 27 c/d blue edge. This means that there are unstable modes in the model with lower frequencies that are not seen in the star. This is, however, a much weaker argument because it is not an uncommon situation that unstable modes are not excited with detectable amplitudes.

Table 2. Possible identifications of the 13 modes detected in XX Pyx. Horizontal lines separate groups of the identifications associated with the consecutive dips of χ^2 seen in Fig. 3. Note that within the group most of the identifications are identical. Models corresponding to each identification are determined by minimalization of χ^2.

	f_6	f_9	f_{12}	f_5	f_{10}	f_{13}	f_4	f_{14}	f_3	f_{11}	f_7	f_2	f_1
	27.003	27.264	28.698	28.995	29.620	31.203	31.392	31.906	33.435	33.637	34.666	36.012	38.110
Model	l n m	l n m	l n m	l n m	l n m	l n m	l n m	l n m	l n m	l n m	l n m	l n m	l n m
D1A	2 3-1	2 3-2	1 5 1	2 4-1	1 5-1	2 5 0	2 5-1	2 5-2	1 6 0	1 6-1	2 6 1	2 6-2	2 7 2
D1B	2 3-1	2 3-2	1 5 1	2 4-2	1 5-1	2 5 0	0 6 0	2 5-2	1 6 0	1 6-1	2 6 1	2 6-2	2 7 2
D1C	2 3-1	2 4 2	1 5 1	2 4-2	1 5-1	2 5 0	2 5-1	2 5-2	1 6 0	1 6-1	2 6 1	2 6-2	2 7 2
D1D	2 3-2	2 4 2	1 5 1	2 4-2	1 5-1	2 5 0	2 5-1	2 5-2	1 6 0	1 6-1	2 6 1	2 6-2	2 7 2
D1E	2 3-1	2 4 2	1 5 1	2 4-2	1 5-1	2 5 0	0 6 0	2 5-2	1 6 0	1 6-1	2 6 1	2 6-2	2 7 2
D1F	2 3-2	2 4 2	1 5 1	2 4-2	1 5-1	2 5 0	0 6 0	2 5-2	1 6 0	1 6-1	2 6 1	2 6-2	2 7 2
D2A	1 4-1	2 3-1	2 4 0	0 5 0	1 5 1	1 5 0	1 5-1	2 5 1	2 5-1	1 6 1	2 6 2	2 6 1	2 6-2
D2B	1 4-1	2 3-2	2 4 0	0 5 0	2 4-2	1 5 0	1 5-1	2 5 1	2 5-1	1 6 1	2 6 2	2 6 1	2 6-2
D2C	1 4-1	2 3-2	2 4 0	2 4-1	2 4-2	1 5 0	1 5-1	2 5 2	0 6 0	2 5-1	1 6 1	2 6 2	2 6-2
D3A	2 3 0	1 4 1	2 4 2	1 4-1	2 4 1	0 5 0	2 4-1	1 5 1	1 5 0	1 5-1	2 5 1	2 5-1	1 6 0
D3B	2 3-1	1 4 1	1 4 0	1 4-1	2 4 1	0 5 0	2 4-1	1 5 1	1 5 0	1 5-1	2 5 1	2 5-1	1 6 0
D3C	2 3-1	1 4 1	2 4 2	1 4-1	2 4 1	0 5 0	2 4-1	1 5 1	1 5 0	1 5-1	2 5 1	2 5-1	1 6 0
D4A	2 3 2	2 3 1	0 4 0	2 3-2	1 4 1	1 4-1	2 4 2	2 4 1	0 5 0	2 4-2	1 5 1	1 5-1	0 6 0
D4B	2 3 2	2 3 1	2 3-1	2 3-2	1 4 1	1 4-1	2 4 2	2 4 1	0 5 0	2 4-2	1 5 1	1 5-1	0 6 0
D5A	1 3 1	2 2-2	1 3-1	2 3 2	2 3 1	2 3-1	0 4 0	2 3-2	1 4 0	2 4 2	2 4 1	2 4 0	1 5 1
D6A	2 2 2	2 2 1	2 2-1	2 2-2	1 3 1	1 3 0	1 3-1	2 3 2	2 3 0	2 3-1	2 3-2	1 4 1	2 4 2
D7A	2 1-2	1 2-1	2 2 2	2 2 1	2 2 0	0 3 0	2 2-2	1 3 1	1 3 0	1 3-1	2 3 1	2 3 0	1 4 1
D7B	2 1-2	1 2-1	2 2 2	2 2 1	2 2 0	0 3 0	2 2-2	1 3 1	1 3-1	2 3 2	2 3 1	2 3 0	1 4 1
D8A	2 1 0	0 2 0	2 1-2	1 2 0	1 2-1	2 2 2	2 2 1	2 2 0	2 2-2	0 3 0	1 3 1	1 3 0	2 3 1

Table 3. Parameters of models determined by the χ^2 minimalization. N_m is the total number of modes with $\ell \leq 2$ within the frequency range of modes detected in XX Pyx. The number decreases with mean density which explains increase of the χ^2 minima. Note that the difference in mean radial mode degree between consecutive groups is close to 0.5. Models used in Fig. 5 are marked with asterisks in the last column.

Model	$M/M_\odot$	$V_{\rm rot}$(ZAMS)	$V_{\rm rot}$	$\log T_{\rm eff}$	$\log L$	$\bar{\rho}/\bar{\rho}_\odot$	χ^2	N_m	$\Sigma(n+l/2)/13$	
D1A	1.9869	57.50	51.92	3.90533	1.2906	.16692	.006876	30	5.92	
D1B	2.0181	61.82	55.92	3.91101	1.3175	.16717	.006217	29	5.92	
D1C	2.0160	60.18	54.43	3.91063	1.3158	.16710	.006224	29	6.00	
D1D	2.0266	59.38	53.69	3.91247	1.3249	.16708	.007508	29	6.00	
D1E	2.0165	61.55	55.69	3.91072	1.3161	.16715	.006108	29	6.00	*
D1F	2.0260	60.59	54.79	3.91235	1.3243	.16711	.007646	29	6.00	
D2A	1.9953	108.01	99.30	3.91241	1.2876	.18680	.008070	27	5.73	*
D2B	2.0477	110.35	101.56	3.92169	1.3320	.18681	.007450	26	5.62	
D2C	2.0333	66.67	61.20	3.92056	1.3233	.18842	.007387	26	5.62	
D3A	1.9122	95.00	88.65	3.90567	1.2064	.21608	.007856	24	5.23	*
D3B	1.9986	97.64	91.16	3.92154	1.2819	.21614	.007181	23	5.23	
D3C	1.9972	95.40	89.09	3.92132	1.2809	.21605	.007530	23	5.23	
D4A	1.8722	66.67	63.00	3.90611	1.1635	.24711	.019895	20	4.77	
D4B	1.8782	67.27	63.60	3.90723	1.1688	.24732	.020005	20	4.77	*
D5A	1.8367	81.32	78.62	3.90907	1.1149	.29872	.036899	19	4.23	*
D6A	1.8527	60.28	59.07	3.92234	1.1148	.36149	.045757	18	3.69	
D7A	1.7556	75.00	74.63	3.90944	1.0074	.41550	.050614	17	3.27	
D7B	1.7562	74.13	73.72	3.90933	1.0086	.41368	.048300	17	3.31	
D8A	1.7500	61.11	61.17	3.91500	0.9819	.48689	.061828	18	2.85	

In Fig. 5 the frequencies determined for XX Pyx are compared with frequencies of low degree modes in selected models. These are not all acceptable but they cover the whole range. The common pattern of the model frequency spectra is the large departure from the equidistant pattern of the rotational splitting. This is particularly well seen in the case of the $\ell = 1$ triplets. One may see that with the increasing radial order the triplet becomes more and more asymmetric, so that the prograde mode $m = -1$ almost overlap the centroid mode $m = 0$ at the high frequency end. There is a near equidistant separation between the consecutive centroid modes at each ℓ in most of the cases. The exception is the low frequency part of the $\ell = 2$ spectrum

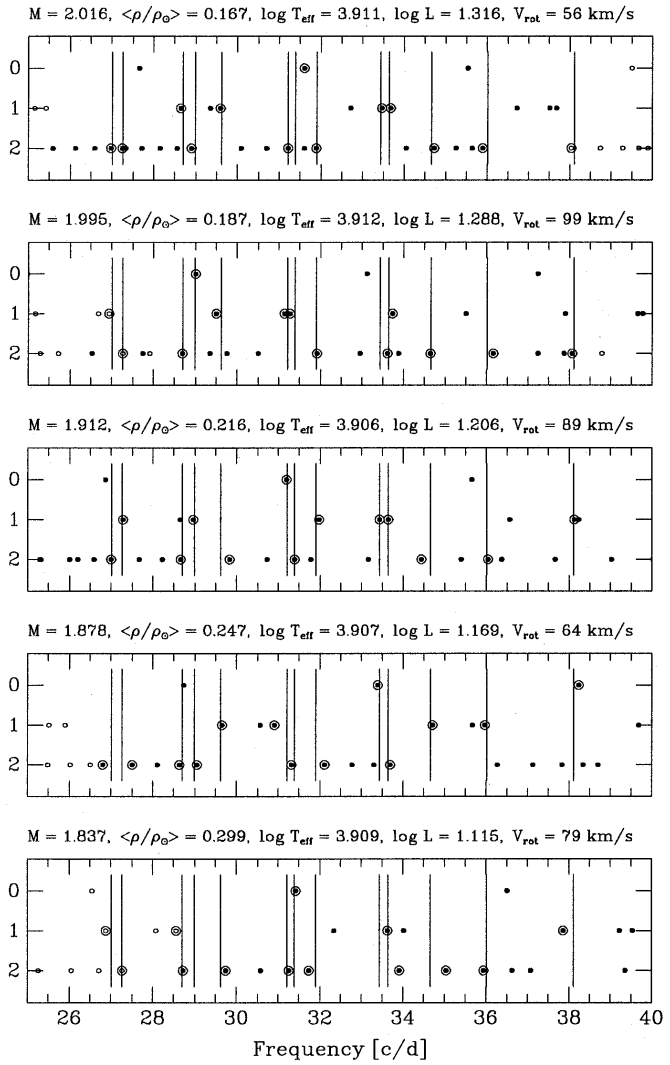

Fig. 5. Comparison of the XX Pyx frequencies (vertical lines) with model frequencies (symbols) for $\ell = 0$ (top row), $\ell = 1$ (middle row), $\ell = 2$ (bottom row). The encircled symbols denote the modes identified with those excited in the star. Small open circles denote the stable modes (always very close to instability $\eta \approx 0$. Positions of the selected models in the H–R diagram are denoted with asterisks in Fig. 4. In Tables 2 and 3 these models (from top to bottom) are denoted as D1E, D2A, D3A, D4B, and D5A.

in all, but the lowest mass models. Here we see the effect of *avoided crossing* between two multiplets. Modes in this range have mixed (p– and g–) character. Their frequencies are sensitive to the structure of the deep interior and therefore these modes are of special interest for seismic sounding.

5.5. Fitting 12 modes

Naturally, if we demand fitting for only 12 of the measured frequencies we may attain significantly lower values of χ^2. To estimate the effect we looked for the minimum of χ^2 considering all possible choices of 12 modes for each model. As expected, the general patterns of the χ^2 dependence on $\bar{\rho}/\bar{\rho}_\odot$ were found very much like those in Fig. 3. In particular, the dips occured at the same locations. For the same set of models the absolute minimum of χ^2 (0.00254) was reached at dip 3 ($\bar{\rho}/\bar{\rho}_\odot = 0.216$). The minimum value was nearly three times smaller than the absolute minimum in the previous 13-mode case. The implied mean frequency mismatch of 0.05 c/d is close to the estimated uncertainty in calculated frequencies. It is, thus, clear that improvement on the side of theory is needed before we will be able to produce a credible seismic model for this star. In the next section we discuss two most needed improvements.

6. Problems

One important effect in the treatment of rotational frequency perturbation which we did not include so far in our calculation was the near–degeneracy of certain modes which may be coupled by rotation. The effect is discussed in details by Soufi et al. (1997). Here we will present selected results for our model D3A.

Uniform (more generally, spherical) rotation couples modes if their azimuthal numbers (m) are the same and their degrees (ℓ) are the same or differ by 2. If the frequency difference between the two (or more) coupled modes is of the order of the rotation frequency one has to use the version of the peturbation formalism appropriate for the case of degeneracy i.e. to consider as a zeroth order basis a linear combination of the nearly degenerate modes. The relative contributions of the components are determined from the second order (in Ω) perturbation equations.

In application to XX Pyx a systematic near–degeneracy occurs between the $\ell = 0$ and 2 modes and between the $\ell = 1$ and 3 modes. In the latter case, for each multiplet we have three coupled modes corresponding to $m = -1$, 0, 1. These near–degeneracies follow from rather high values of n and, hence, approximate validity of the p–mode asymptotics. We also considered coupling involving three modes, e.g. $\ell = 0$, 2, 4 or $\ell = 0$, 2, 2, in the case of avoided crossing. In none of the cases considered the inclusion of the third mode was essential.

Model D3A and its oscillation frequencies were obtained by means of interpolation described in the previous section. In order to evaluate the effect of the degeneracy we had to recalculate the model and its frequencies. A comparison of the two upper panels of Fig. 6 clearly shows that the grid of models was not sufficiently dense. The differences between interpolated and calculated frequencies are easily seen, especially for the $\ell = 2$ modes near the avoided crossing. This inadequacy of our grid is not essential at this stage but must be kept in mind in more advanced efforts. In the top panel one may see how the fit is improved if the $\ell = 2$ identification for $f_7 = 34.7$ c/d is replaced with the $\ell = 3$. The value of χ^2 is then lowered by some 30 %. No fit improvement is achieved by allowing the $\ell = 3$ identification for another poorly fit frequency $f_{10} = 29.6$ c/d. One may see, however, in the mid panel that the situation changes if instead of the interpolated frequencies one uses the calculated ones.

A comparison of the mid and bottom panels shows the effect of the coupling between nearly degenerate modes. The effect is

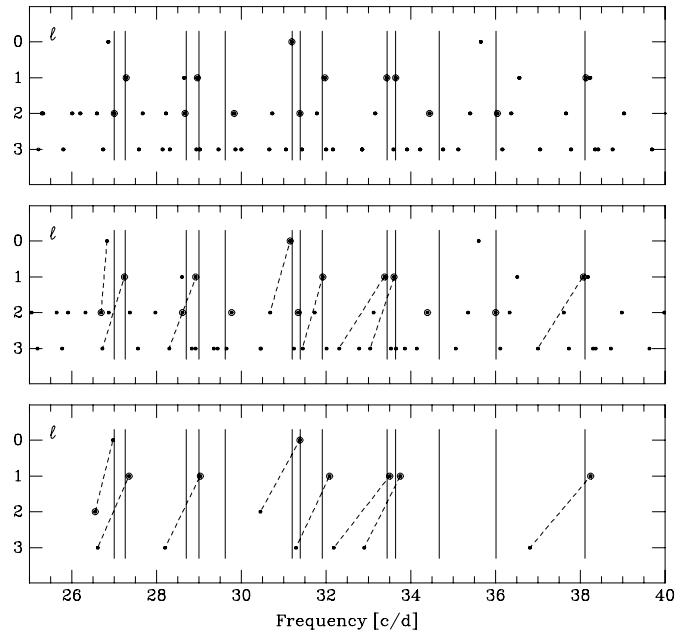

Fig. 6. Effects of inadequate grid density and near degeneracy shown for one of the best models (D3A). The upper panel shows interpolated frequencies which are the same (except that $\ell = 3$ modes are added) as in the mid panel in Fig. 5. The mid panel here shows frequencies of the same modes for the recalculated model. Frequencies of the modes coupled by rotation are connected with dashed lines. The resulting frequencies of these modes are shown in the lower panel.

Table 4. Effects of coupling between nearly degenerate modes

$f_{\rm obs}$	ℓ	n	m	f_0	δf	$A_{\rm low}$	$A_{\rm high}$
f_6	0	4	0	26.832	0.139	0.923	-0.385
	2	3	0	26.686	-0.139	0.761	0.649
f_9	1	4	1	27.239	0.112	0.935	-0.356
	3	3	1	26.720	-0.112	0.422	0.906
f_5	1	4	-1	28.932	0.096	0.951	-0.308
	3	3	-1	28.293	-0.096	0.374	0.927
f_{13}	0	5	0	31.153	0.226	0.881	-0.474
	2	4	0	30.678	-0.226	0.513	0.858
f_{14}	1	5	1	31.923	0.153	0.915	-0.403
	3	4	1	31.443	-0.153	0.481	0.877
f_3	1	5	0	33.374	0.122	0.962	-0.275
	3	4	0	32.302	-0.122	0.337	0.942
f_{11}	1	5	-1	33.613	0.137	0.931	-0.365
	3	4	-1	33.038	-0.137	0.441	0.897
f_1	1	6	0	38.064	0.174	0.944	-0.329
	3	5	0	36.988	-0.174	0.370	0.929

best seen in the case of $\ell = 2$ and 0 modes. The frequency distance between the modes increases when the coupling is taken into account. In Table 4 we give the values of the frequency shifts (δf) caused by the mode coupling as well as the amplitudes of the spherical harmonic components ($A_{\rm low}$ is corresponding to $\ell = 0$ or 1 and $A_{\rm high}$ is corresponding to $\ell = 2$ or 3). One may see that the mutual contamination of the $\ell = 0$ and 2 components is quite strong. This is bad news for prospects of mode discrimination by means of two–color photometry because such contaminated modes may appear in the *amplitude ratio – phase difference* diagrams (Watson 1988, Garrido et al. 1990) in the $\ell = 0$, 1 or 2 domains depending on the inclination of the rotation axis. Fortunately, modes with $m \neq 0$ are not affected. The mutual contamination is also significant for the $\ell = 1$ and 3 pairs. In all the cases the nominal $\ell = 3$ modes will be most likely observable through their $\ell = 1$ contaminations.

7. Discussion

Clearly, we have not succeeded in constructing the seismic model of XX Pyx. Models regarded as plausible, such as those in Fig. 5, do not reproduce the frequencies within the observational errors. In fact, we are quite far from the $10^{-3} - 10^{-2}$ c/d error range seen in Table 1. The departures from the fit for some of the identifications are in fact easily visible in Fig. 5. The problem proved more difficult than we have anticipated. We believe that we learned something in the process and that this knowledge should be shared with other groups undertaking similar efforts.

Undoubtedly, an improvement of the fits could be accomplished by allowing adjustment of the chemical composition parameters. The overshooting distance and parameters in the radial dependence of rotation rate should also be regarded as adjustable quantities. These degrees of freedom affect primarily the positions of the mixed modes relative to pure p–modes. In this application the mixed modes exist for $\ell = 2$ at the low frequency end. Such modes extend to higher frequencies for higher ℓ's. However, the freedom allows also a fine tuning of the distances between pure p–modes. One could hope that there is just one mode identification and one corresponding model of the star for which the frequency fit within the measurement errors is possible.

The reason why we cannot yet proceed this way is that our treatment of rotation is not adequate. We used here a perturbation theory which is accurate up to some 0.05 c/d, much worse than the measurement accuracy. We are not yet sure that the recently developed cubic theory (Soufi et al. 1997) would yield a sufficient accuracy.

Observational determination of the ℓ values for some of the excited modes could significantly change the situation. Imagine, for instance, that we find that the photometric data place the f_1 mode into the $\ell = 0$ domain of an *amplitude ratio – phase difference* diagram (see Watson 1988, Garrido et al. 1990). We may see in Table 1 that this mode has far the highest amplitude and certainly it will be the first for which we will have the required data. As we have discussed in Sect. 6, the possibility that this is not a $\ell = 0$ mode but rather a $\ell = 2, m = 0$ mode must be considered. Fortunately, we do not see such an identification for f_1 in Table 2. Thus, we are left with only two models, D4A and D4B, with very similar parameters and the same identification for almost all modes excited in XX Pyx. We could discriminate between the two if we knew ℓ for f_{12} which is the only mode with different identification. If, however, the

f_1 position in the diagram corresponds to an $\ell = 1$ domain, we are less lucky. The possible models are not only six models with $\ell = 1$ for f_1 but also models D4A and D4B with $\ell = 0$ because radial modes contaminated with a $\ell = 2$ component may appear in the $\ell = 1$ domain. The ambiguity implies a wide range of admissible model parameters.

Acknowledgements. Pamyatnykh and Dziembowski enjoyed the hospitality during their stays in Vienna and express their thanks to Mike Breger and his collaborators for it. We all thank Bohdan Paczyński, Maciej Kozlowski and Ryszard Sienkiewicz for the stellar evolution code. We thank also Marie–Jo Goupil for her contribution to development of the code calculating the rotational splitting. This work was supported in part by the Austrian Fonds zur Förderung der wissenschaftlichen Forschung, project number S7304, and also by the grants AFOSR–95–0070, NSF–INT–93–14820, RFBR–95–02–06359 and KBN–2P304–013–07.

References

Bahcall, J. N., Pinsonneault, M. H. 1995, Rev. Mod. Phys, 67, 781
Breger, M., 1997, in *New eyes to see inside the Sun and stars: pushing the limits of helio– and asteroseismology with new observations from ground and from space*, Proc. IAU Symp. 185, Kyoto, in press
Breger, M., Handler, G., Nather, R. E., et al. 1995, A&A, 297, 473
Breger, M., Zima, W., Handler, G., et al. 1997, A&A, in press
Christensen–Dalsgaard, J., Däppen, W. 1993, A&AR, 4, 267
Cugier, H., Dziembowski, W. A., Pamyatnykh, A. A. 1994, A&A, 291, 142
Dziembowski, W. A. 1977, Acta Astron., 27, 203
Dziembowski, W. A., Goode, P. R. 1992, ApJ, 394, 670
Garrido, R., Garcia–Lobo, E., Rodriguez, E. 1990, A&A, 234, 262
Goupil, M.–J., Michel, E., Lebreton, Y., Baglin, A. 1993, A&A, 268, 546
Goupil, M.–J., Dziembowski, W. A., Goode, P. R., Michel, E. 1996, A&A, 305, 487
Grevesse N., Noels A. 1993, in *Origin and Evolution of the Elements*, eds. Pratzo N., Vangioni-Flam E., Casse M., Cambridge Univ. Press., p. 15
Guzik, J. A., Bradley, P. 1995, Baltic Astronomy, 4, 442
Handler, G., Breger, M., Sullivan, D. J., et al. 1996, A&A, 307, 529
Handler, G., Pikall, H., O'Donoghue, D., et al. 1997a, MNRAS, 286, 303 (HPO)
Handler, G., Pamyatnykh, A. A., Zima, W., et al. 1997b, MNRAS, in press
Iglesias, C. A., Rogers, F. J. 1996, ApJ, 464, 943
Kurtz, D. W., 1983, IBVS 2285
Mantegazza, L., Poretti, E., Bossi, M. 1996, A&A, 308, 847
Paczyński, B. 1969, Acta Astron., 19, 1
Paczyński, B. 1970, Acta Astron., 20, 47
Rogers, F. J., Iglesias, C. A. 1994, Sci, 263, 50
Rogers, F. J., Swenson, F. J., Iglesias, C. A. 1996, ApJ, 456, 902
Seaton, M. J., 1996, MNRAS, 279, 95
Soufi, F., Goupil, M.–J., Dziembowski, W. A., 1997, A&A, submitted
Unno, W., Osaki, Y., Ando, H., Saio, H., Shibahashi, H. 1989, Nonradial oscillations of stars, University of Tokyo Press
Watson, R. D. 1988, Ap&SS, 140, 255